Enhancement of the formation of the $C54$ phase of $TiSi_2$ through the introduction of an interposed layer of tantalum

A. Mouroux,* S.-L. Zhang, and C. S. Petersson
Department of Electronics, Royal Institute of Technology-Electrum, Box E229, S-164 40 Kista, Sweden
(Received 16 December 1996)

When annealing a Ti/Mo bilayer deposited on Si substrate, a layer of $(Mo,Ti)Si_2$ forms first and then acts as a template for the growth of the $C54$ phase of $TiSi_2$ at 650 °C that is about 100° lower than what is usually needed for the $C49-C54$ phase transformation. We show in this paper that using Ta instead of Mo as the interposing layer between Ti and Si also leads to the formation of the $C54$ phase apparently without going through the otherwise usual sequence for the formation of $TiSi_2$, i.e., the $C49$ phase forms as a result of the Ti-Si interaction and the $C54$ phase forms as the product of phase transformation. The choice of Ta here is based on simple crystallographic considerations; the in-plane lattice mismatch between the basal planes of the hexagonal $TaSi_2$ phase and the $\langle 010 \rangle$ planes of the $C54$ phase is within 0.3%, a factor of 10 times better than that between the basal planes of the hexagonal $(Mo,Ti)Si_2$ phase and the $\langle 010 \rangle$ planes of the $C54$ phase. No ternary phase seems to form in the Ta-Ti-Si ternary system, and Si is the dominant diffusion species in both binary systems Ta-Si and Ti-Si. Hence, the formation of the hexagonal $TaSi_2$ phase at the interface between Ti and Si is expected to be straightforward without complications. The template growth of the $C54$ phase is found unaffected by varying the conditions used for the metal deposition. The present results with Ta as well as with Mo confirm that the template mechanism is responsible for the enhanced formation of the $C54$ phase of $TiSi_2$. [S0163-1829(97)00240-3]

I. INTRODUCTION

The formation of $TiSi_2$ is of great importance not only for practical applications in the microelectronics industry, but also for the fundamental understanding of the phase formation of intermetallic compounds. $TiSi_2$ may exist either as the base-centered orthorhombic $C49$ phase (with a resistivity of 60–70 $\mu\Omega$ cm) or as the face-centered orthorhombic $C54$ phase (with a lower resistivity of 15–20 $\mu\Omega$ cm).[1,2] Usually, the $C49$ phase forms first as a result of Ti-Si interaction at 300–550 °C; and then, the $C54$ phase forms at around 700 °C as the product of the $C49-C54$ phase transformation. As the low-resistivity stable $C54$ phase is desired, one of the main issues with the conventional self-aligned silicide process, used for the formation of $TiSi_2$ for applications in very-large-scale-integration technology, concerns specifically the $C49-C54$ transformation. This is particularly the case for metallization of devices with dimensions below 0.3 μm.[3] It is well established that the temperature required for the $C49-C54$ transformation increases with increasing dopant concentration in Si,[4] decreasing thickness of the preformed $C49$ phase,[5] or decreasing linewidth.[6–8] In spite of numerous intensive studies, the formation of $TiSi_2$ is not completely understood. Alternative methods of forming the $C54$ phase have been actively searched for.[9]

It has been shown recently that the temperature needed for the formation of the $C54$ phase can be lowered by 100–150°, either by ion implantation of Mo or W to a dose as small as 10^{13} ions/cm^2 into Si substrates prior to Ti sputter deposition,[10] or by deposition of a thin Mo layer of about 1 nm thickness between Ti films and Si substrates.[11–13] The dependence of the transformation temperature on linewidth is also greatly reduced in the presence of Mo.[14,15] The enhanced formation of the $C54$ phase by the Mo or W ion implantation is interpreted resulting from the increased number of active triple junctions in the $C49$ phase where the $C54$ phase nucleates.[10] The enhanced growth of the $C54$ phase by the interposition of a Mo layer is, however, attributed to the formation of a layer of the Mo-Ti-Si ternary phase of hexagonal structure, i.e., $(Mo,Ti)Si_2$, between the remaining Ti films and the Si substrates.[11,12] Once formed, the $(Mo,Ti)Si_2$ layer acts as a template for the growth of the $C54$ phase. The in-plane lattice mismatch between the basal (i.e., $\langle 001 \rangle$) planes of the hexagonal $(Mo,Ti)Si_2$ phase[16,17] and the $\langle 010 \rangle$ planes of the $C54$ phase[18] is within 3%.

If the template growth is the true mechanism responsible for the enhanced formation of the $C54$ phase, a system different from Mo-Ti-Si can also be considered. According to simple crystallographic considerations,[19] either Ta or Nb can be used to replace Mo as the interposing layer between Ti and Si, since both $TaSi_2$ (Ref. 20) and $NbSi_2$ (Ref. 21) have an identical crystallographic hexagonal structure as $(Mo,Ti)Si_2$ with an even better in-plane lattice match between their basal planes and the $\langle 010 \rangle$ planes of the $C54$ phase. An added advantage of using the Ti/Ta/Si or Ti/Nb/Si structures is that the formation of hexagonal phase $TaSi_2$ or $NbSi_2$ at the interface between Ti and Si is anticipated to be straightforward without complications, since the ternary phase, if it exists, in either a Ta-Ti-Si or Nb-Ti-Si ternary system, does not form at the temperature of interest.[22–25] Moreover, Si is the dominant diffusion species in all the relevant binary metal-Si systems in the two ternary systems being considered here.[26]

In the present work, the effect of an interposed Ta layer on the formation of $TiSi_2$ is first investigated. It will be shown that Ta indeed has the same effect as Mo in enhancing

the formation of the *C*54 phase via the template mechanism. The impact of interfacial impurities on the formation of the silicides will then be studied by varying the conditions for the deposition of the Ti/Mo bilayers.

II. EXPERIMENT AND ANALYSIS

The substrates used in this work were always Si wafers of ⟨100⟩ orientation, 100 mm in diameter, lightly boron-doped with a resistivity of about 10 Ω cm. Prior to metal deposition, the wafers were cleaned following the standard wafer-cleaning procedure which ended with native oxide removal by a short immersion in diluted HF ($HF:H_2O=1:10$) and then were water-rinsed and spin dried. Three different metal depositions were carried out in a dual source electron-beam evaporator: one with 60 nm Ti as control, one with a bilayer of 60 nm Ti on top of 0.5 nm Mo, and one with a bilayer of 60 nm Ti on top of 0.5 nm Ta. All thickness values are nominal ones. For the bilayer depositions, the metals were deposited consecutively without breaking the vacuum. The base pressure in the evaporator was 2×10^{-7} Torr. The vacuum chamber was always first purged with N_2 and then pumped down to the base pressure before metal deposition. In order to study how impurities could affect the silicide formation, no N_2 purge was made for some depositions where the time spent for pumping down the chamber to base pressure was considerably longer. Annealing, from 600 to 750 °C for 30 s was performed in N_2 with an AG Associates Heatpulse Rapid Thermal Annealing (RTA) system. Silicide formation was monitored *ex situ* by sheet resistance measurement using a four-point probe. To facilitate the resistance measurement of the silicide layers, unreacted metals as well as any surface TiN formed during RTA were removed selectively by immersing the wafers sequentially in $H_2O_2:H_2SO_4$ (1:4) at 90 °C for 10 min. and then in $NH_4OH:H_2O_2:H_2O$ (1:1:5) at 40 °C for 10 min, followed by a water rinse and spun drying. The layer configuration, thickness and composition were determined by Rutherford backscattering spectrometry (RBS) with $^+$He ions at an acceleration energy of 2.4 MeV. A θ-2θ (Bragg-Brentano geometry) x-ray diffractometer (XRD) equipped with a Cu tube and a post-sample monochromator was employed to identify phase formation and to study crystallographic orientation. Cross-sectional transmission electron microscopy (TEM) was used to study local morphology of the silicide layers as well as to provide lattice images of the silicides formed. Depth profiling of the elements involved in the metal-Si systems was carried out using secondary-ion mass spectrometry (SIMS).

III. RESULTS AND DISCUSSION

A. Influence of Ta on the formation of the *C*54 phase

Figure 1 shows the variations of sheet resistance of the silicide layers versus the annealing temperature used for the formation of the silicide. The (equivalent) thickness of the Ta layer is 1.33 nm and that of the Ti layer 87 nm, calculated from the RBS spectra with the bulk density of the respective metals. It is seen clearly in the figure that Ta has the same effect as Mo on the reduction of the sheet resistance of the silicide layers formed at 650 °C and above. Only after annealing at 750 °C, the sheet resistance of the silicide formed

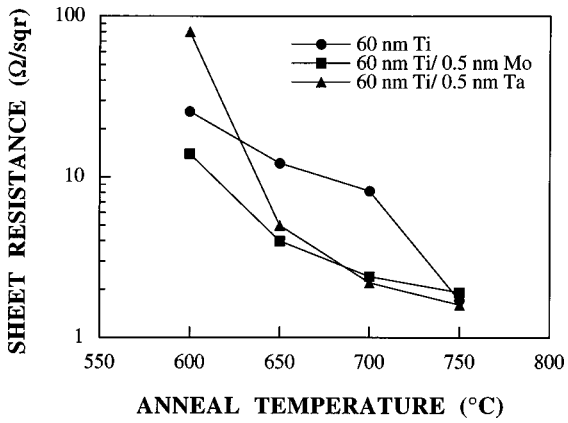

FIG. 1. Sheet resistance of the silicide layers formed with the different metal systems deposited on the ⟨100⟩ Si substrates as a function of anneal temperature. The sheet resistance was measured after selective removal of unreacted metals and surface TiN by wet chemical etching.

on the control wafer with pure Ti reaches the same low value as the two wafers with either Ti/Mo or Ti/Ta bilayer. The *y* axis of the figure, i.e., sheet resistance in Ω per square, is in the logarithmic scale.

In order to understand the variation of the sheet resistance depicted in Fig. 1, the wafers were analyzed with XRD; the results (partial spectra from 38 to 44°) are shown in Fig. 2. The *y* axis of the figure, i.e., intensity in counts per second (c/s), is also in logarithmic scale to display weak diffraction peaks while still showing the full features of intense ones. At 600 °C, only the *C*49 phase of $TiSi_2$ is found on the control wafer, evidenced by the *C*49 (131) peak at $2\theta=41.2°$ shown in Fig. 2(a). At the same temperature, the ternary hexagonal $(Mo,Ti)Si_2$ phase forms in the presence of Mo [see the broad peak at about $2\theta=41.5°$ in Fig. 2(b), which is assigned to (003) of $(Mo,Ti)Si_2$], in agreement with our previous results.[11] However, phase formation cannot be concluded by XRD for the wafer with a Ta interposing layer and annealed at 600 °C, cf. Fig. 2(c). These results are in accordance with the sheet resistance data shown in Fig. 1; for the Ti/Ta/Si structure, the sheet resistance is the highest among those three wafers annealed at 600 °C.

Raising the annealing temperature to 650 °C does not change the phase formed on the control wafer, except that the intensity of the *C*49 (131) diffraction peak is now increased by a factor of about 3 [Fig. 2(a)]. The formation of the *C*54 phase of $TiSi_2$ is evident on the wafer with a Mo layer, as two diffraction peaks of this phase are detected unambiguously, i.e., (040) at about $2\theta=42.4°$ and (022) at about $2\theta=43.4°$, together with the $(Mo,Ti)Si_2$ (003) peak [Fig. 2(b)]. On the wafer with a Ta layer, a diffraction peak at about $2\theta=40.3°$ is detected and assigned to (111) of the hexagonal $TaSi_2$ phase. However, the *C*54 phase is not found according to XRD [Fig. 2(c)], which appears inconsistent with the resistance measurement results which indicate the formation of this phase (Fig. 1). The discrepancy between the XRD results and the sheet resistance data will be discussed later.

Increasing the annealing temperature further to 700 °C does not change the basic features of the silicide formation with only one exception: the *C*54 phase now becomes de-

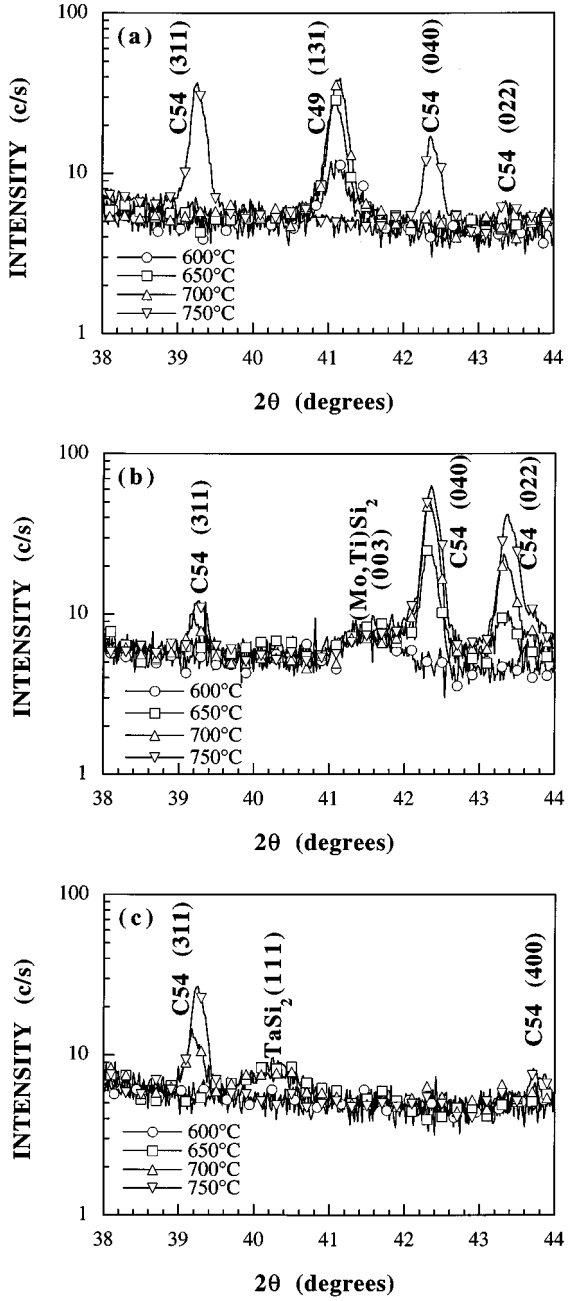

FIG. 2. Diffraction patterns of the silicide(s) formed at various temperatures (a) on the control wafers with pure Ti, (b) on the wafers with the Ti/Mo bilayers (deposited with the N_2 purge), and (c) on the wafers with the Ti/Ta bilayers.

tectable together with the $TaSi_2$ (111) peak on the wafer with Ta [see the $C54$ (311) peak at about $2\theta = 39.3°$ in Fig. 2(c)]. However, the intensity of this peak seems to be too weak to account for the amount of the $TiSi_2$ formed as can be conceived from the corresponding resistance value in Fig. 1.

When annealed at 750 °C, the $C49$ phase is converted to the $C54$ phase for the entire $TiSi_2$ layer on the control wafer [Fig. 2(a)]. The $C49$–$C54$ phase transformation completes in a very narrow temperature window ($\sim 50°$), typical of such processes controlled kinetically by nucleation.[27] On the other hand, no fundamental changes can be observed for the silicides formed on the wafers with an interposed layer of either

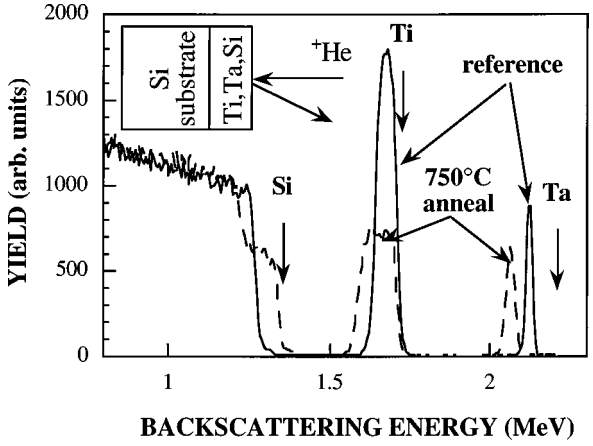

FIG. 3. RBS spectra showing the growth of $TiSi_2$ on top of $TaSi_2$, as can be concluded by the energy position of the Ta peak for the wafer annealed at 750 °C. For the annealed wafer, unreacted metals and surface TiN were selectively removed.

Mo or Ta. For the case with Mo, the $C54$ (220) peak begins to become comparable (in intensity) with the (040) peak, Fig. 2(b). For the case with Ta, the (311) peak of the $C54$ phase continues to increase in intensity, but the $TaSi_2$ (111) peak seems to disappear altogether from the spectrum in Fig. 2(c). As the hexagonal $TaSi_2$ is the stable phase in the temperature range studied in the presence of excess Si, the disappearance of the $TaSi_2$ (111) peak in the XRD spectrum can only be attributed to a slight change in the crystallographic orientation of the $TaSi_2$ crystals with reference to the wafer normal. The $(Mo,Ti)Si_2$ and $TaSi_2$ layers formed are both found to be strongly textured but with different preferential orientations. The former has a clear ⟨001⟩ texture and the latter tends to have a ⟨111⟩ orientation. Thus, alignment of the crystallographic orientations of the crystals in these layers in relation to the wafer normal is important for the XRD analysis. This is considered to be the reason also for the undetectable $C54$ (311) peak for the wafer annealed at 650 °C. How the preferential orientation of $TaSi_2$ will influence the texture of the $C54$ phase subsequently grown on its top will be made clear below.

What is significant with the results above is the apparent suppression of the formation of the $C49$ phase of $TiSi_2$ with the presence of an interposed layer of either Mo or Ta. As in the case of Mo,[11] the $TaSi_2$ is found to remain at the interface between the $C54$ phase and the Si substrate during the growth of $TiSi_2$, according to the RBS results shown in Fig. 3. How $TaSi_2$ enhances the formation of the $C54$ phase of $TiSi_2$ is discussed as follows.

The in-plane lattice mismatch between the basal planes of the hexagonal $TaSi_2$ phase and the ⟨010⟩ planes of the $C54$ phase is within 0.3%, 10 times better than that between the basal planes of the hexagonal $(Mo,Ti)Si_2$ phase and the ⟨010⟩ planes of the $C54$ phase.[11,12] Therefore, it is reasonable to suggest that the hexagonal $TaSi_2$ phase, like the hexagonal $(Mo,Ti)Si_2$ phase, also acts as a template for the formation of the $C54$ phase of $TiSi_2$ already at 650 °C. According to Fig. 4, the angle between the ⟨111⟩ and ⟨001⟩ planes of the hexagonal $TaSi_2$ is 70° (left sketch), and that between the ⟨311⟩ and ⟨010⟩ planes of the $C54$-$TiSi_2$ is 74.4° (right sketch). Thus, matching the ⟨010⟩ planes of the $TiSi_2$ with the ⟨001⟩

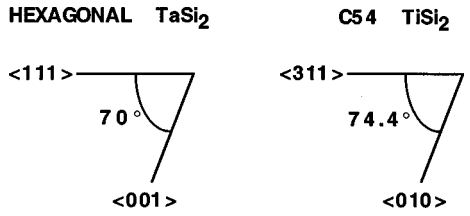

FIG. 4. Schematic presentation of the angular relationship between the ⟨111⟩ and ⟨001⟩ crystallographic planes of the hexagonal $TaSi_2$ phase (left sketch) and the ⟨010⟩ and ⟨311⟩ crystallographic planes of the *C*54 phase of $TiSi_2$ (right sketch).

planes of the $TaSi_2$, equivalent to epitaxial growth of the $TiSi_2$ on the $TaSi_2$, will give rise to a small angle of 4.4° between the ⟨311⟩ planes of the former phase and the ⟨111⟩ planes of the latter one. The simultaneous observation of the (111) peak of $TaSi_2$ and the (311) peak of the *C*54 phase in Fig. 2(c) is then considered as a consequence of the epitaxial alignment of the ⟨010⟩ planes of the *C*54 phase towards the ⟨001⟩ planes of the hexagonal $TaSi_2$ phase.

The epitaxial growth of transition-metal silicides on Si substrates has been systematically studied.[28] On a clean Si surface, hexagonal $MoSi_2$ can grow epitaxially on ⟨100⟩ Si with the normal of its basal planes parallel to Si ⟨100⟩. Thus, (Mo,Ti)Si_2 may also grow epitaxially on ⟨100⟩ Si either via $MoSi_2$ or directly, as (Mo,Ti)Si_2 and $MoSi_2$[29] differ very little in their lattice parameters. Hence, it is the epitaxial planes that are observed in Fig. 2(b) for the Ti/Mo/Si structures, i.e., the (Mo,Ti)Si_2 (003) peak as well as the *C*54 (040) peak. As the epitaxial growth of hexagonal $TaSi_2$ on ⟨100⟩ Si occurs under different conditions from $MoSi_2$,[28] it can be understood that different diffraction peaks are observed on the $TiSi_2$/$TaSi_2$ silicide bilayers [Fig. 2(c)]. The observation of the *C*54 (311) peak relies on the epitaxial alignment of another crystallographic orientation (i.e., ⟨010⟩) towards the ⟨001⟩ orientation of the underlying $TaSi_2$. The angle of 4.4° between the ⟨111⟩ planes of $TaSi_2$ and the ⟨311⟩ planes of $TiSi_2$ (Fig. 4) is thus concluded to be responsible for the failure (a) to detect the $TiSi_2$ (311) peak on the wafer annealed at 650 °C and (b) to detect the $TaSi_2$ (111) peak on the other wafer annealed at 750 °C, i.e., Fig. 2(c). That the $TaSi_2$ layers tend to be preferentially oriented towards ⟨111⟩ instead of the reported[28] ⟨110⟩, ⟨124⟩, or ⟨122⟩ may depend on the conditions used for the deposition of the Ti/Ta bilayers.

B. Influence of interfacial impurities on the formation of the *C*54 phase

The preparation of the metal layers has an important bearing on the growth of the silicide layers. Figure 5 shows the XRD results of the silicide formation from the Ti/Mo bilayers deposited without purging the vacuum chamber with N_2. They will be denoted as samples B hereafter, in opposition to the previously analyzed samples A. The $TiSi_2$ layers grown are again only composed of the *C*54 phase according to XRD and sheet resistance measurement (below). But they are characterized with a ⟨311⟩ preferential orientation, similar to the $TiSi_2$ layers formed from the Ti/Ta bilayers [Fig. 2(c)] but different from those formed from the ''clean'' Ti/Mo bilayers deposited after purging the chamber with N_2

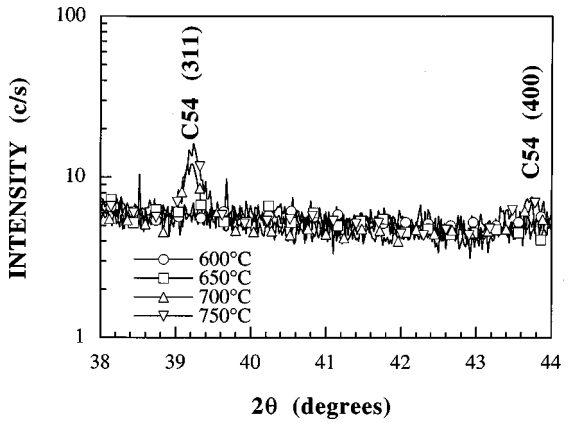

FIG. 5. Diffraction results depicting the formation of the *C*54 phase of $TiSi_2$ with the Ti/Mo bilayers deposited without the N_2 purge (denoted as samples B).

(denoted as samples A hereafter) [Fig. 2(b)]. Further, the ternary (Mo,Ti)Si_2 phase is not found in Fig. 5.

The preferred ⟨311⟩ orientation of the *C*54 phase on samples B is confirmed by the cross-sectional TEM analysis of these wafers. As seen in Fig. 6(a), the $TiSi_2$ layer formed at 750 °C is characterized with a very smooth surface and flat interface with the Si substrate. On Fig. 6(b), the lattice image of the *C*54 phase is shown and the distance between two adjacent columns of atoms is found to be about 0.365 nm. This value coincides precisely with the interplanar distance for the ⟨111⟩ planes of the *C*54 phase, i.e., 0.373 nm.[18] The angle between the horizontal line (e.g., along the $TiSi_2$-Si interface) and these atomic columns is measured to be around 30°, which corresponds to the angle between the ⟨111⟩ and ⟨311⟩ planes of the *C*54 phase. Thus, the ⟨311⟩ planes are parallel to the sample surface and are detectable by XRD (in the present diffraction geometry). The angular relationship illustrated for $TaSi_2$ in Fig. 4 is also quite valid for (Mo,Ti)Si_2. That the (111) peak of (Mo,Ti)Si_2 is not found in Fig. 5 is interpreted as resulting from the very small amount of this hexagonal phase with the very low scattering efficiencies of the Mo and Ti atoms as compared with that of the Ta atoms. In addition, the ⟨111⟩ orientation of the (Mo,Ti)Si_2 crystals may also be slightly off from the wafer normal.

The sheet resistance measurement results from samples B are depicted in Fig. 7. For the sake of comparison, the resistance results from samples A as well as those from the silicide layers formed on the control wafers are also included in the figure. The resistivity, with the thickness information obtained from the RBS measurement, of the $TiSi_2$ layers is 16.3 $\mu\Omega$ cm for the silicides formed on samples B. This value is slightly higher than those of the silicide layers formed on samples A (15.2 $\mu\Omega$ cm) and formed with the Ti/Ta bilayers (14.5 $\mu\Omega$ cm), but quite comparable with that of the silicide layers formed on the control wafers without either Mo or Ta (16.6 $\mu\Omega$ cm). Nevertheless, these low-resistivity values provide immediate evidence of the formation of the *C*54 phase of $TiSi_2$ at 650 °C with an interposed layer of Mo or Ta, despite the difference in the preparation procedures (with and without chamber purging with N_2) prior to the deposition of the Ti/Mo bilayers.

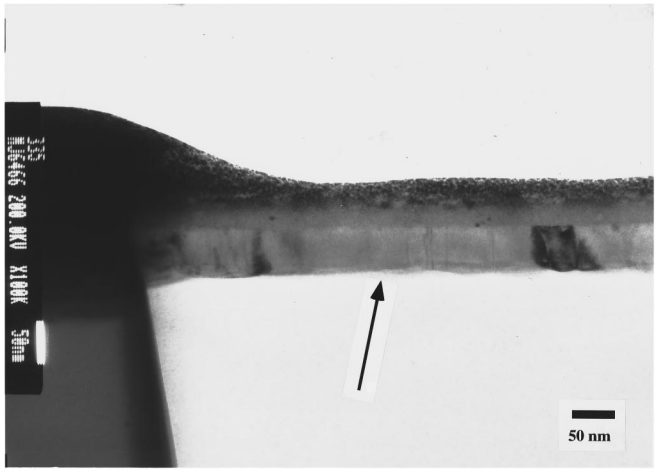

(a)

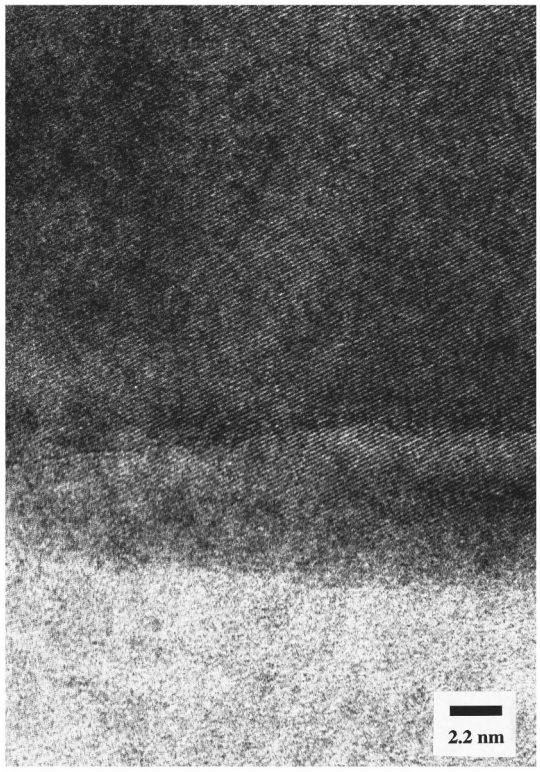

(b)

FIG. 6. Cross-sectional TEM pictures of the $TiSi_2$ formation at 750 °C with the Ti/Mo bilayers deposited without the N_2 purge (samples B). The surface TiN is kept unetched. Besides, a Pt layer was deposited on top of the sample surface in order to protect the silicide layers during the sample preparation for TEM. (a) The $TiSi_2$ has a smooth surface and a flat interface to the Si substrate. (b) Lattice image of the section indicated by the arrow in (a) shows the atomic columns of the ⟨111⟩ planes of the *C*54 phase of $TiSi_2$. The ternary (Mo,Ti)Si_2 phase between $TiSi_2$ and Si substrate is however too thin to reveal.

The sheet resistance of samples B is consistently higher than that of samples A (Fig. 7). This difference in sheet resistance results mainly, according to RBS, from the difference in the thickness of the $TiSi_2$ (*C*54 phase) layers formed. For instance, the $TiSi_2$ layer is 95 nm thick on samples A but only 63 nm on samples B after annealing at 750 °C. The

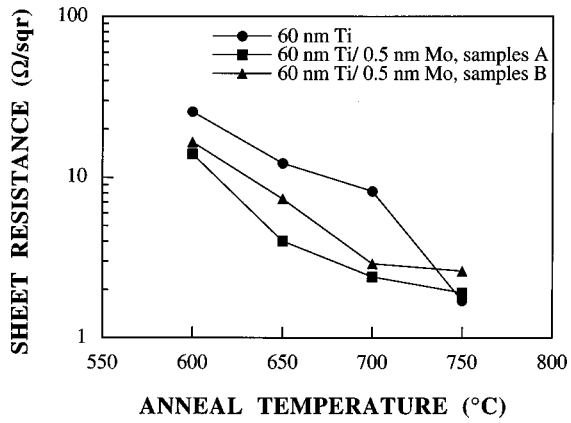

FIG. 7. Sheet resistance of the silicide layers formed with the Ti/Mo bilayers deposited on the ⟨100⟩ Si substrates with (samples A) and without (samples B) the N_2 purge. The resistance results of the silicide layers formed on the control wafers are also shown for comparison. As in Fig. 1, the sheet resistance was measured after selective removal of unreacted metals and surface TiN by wet chemical etching.

SIMS depth profiling of these two particular samples also shows clearly this thickness difference, Fig. 8 (with the surface TiN layers being kept unetched); the displacement of the Mo peak towards longer sputtering time for samples A indicates a thicker $TiSi_2$ layer formed on top of it, as compared with the $TiSi_2$ layer on samples B. However, whether purging with N_2 has any influence on the growth rate of the *C*54 phase cannot be concluded here, since the thickness of the initial Ti layers is different for these wafers, 83 nm for samples A and 58 nm for samples B.

It is now established that purging of the chamber with N_2 not only affects the resistivity of the $TiSi_2$ layers grown but also has a noticeable impact on the preferential orientation of the (Mo,Ti)Si_2 and *C*54 phases formed. The thickness of the

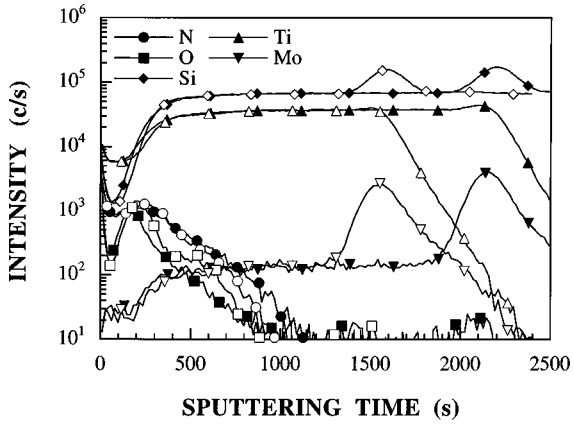

FIG. 8. SIMS depth profiling showing the distribution of the elements involved in the systems after the silicide formation at 750 °C, with the Ti/Mo bilayers deposited with (samples A, filled symbols) and without (samples B, open symbols) the N_2 purge. The surface TiN is kept unetched. The displacement of the Mo peak towards longer sputtering time indicates more $TiSi_2$ formed on samples A than on samples B, under the same conditions for the silicidation anneal. It is worthwhile to point out that the oxygen level at the interface between the silicide and the Si is below the detection limit of SIMS for both samples.

Mo layers deposited is 0.76 nm for samples A and 0.52 nm for samples B, according to RBS. However, the variation of the Mo thickness from 0.5 to 2.0 nm does not influence the growth of the ⟨001⟩-oriented hexagonal $(Mo,Ti)Si_2$ and then the ⟨010⟩-oriented $C54$ phase of $TiSi_2$.[11] Moreover the initial Ti thickness cannot make such a difference in the silicide formation in terms of the resistivity and preferential orientation of the $TiSi_2$ layers.[12] Thus, it is suggested that other factors, possibly interfacial oxygen including the oxygen in native oxide and the oxygen incorporated in the deposited Mo layers, are responsible for the difference in the silicide formation on samples A and samples B.

As Mo cannot reduce SiO_2,[30] the presence of interfacial oxygen can hinder the diffusion of Si towards the metal layers to form $(Mo,Ti)Si_2$ and $TiSi_2$. Interfacial oxygen can, however, be removed from the interface once it is in contact with Ti at the annealing temperatures used.[30] This may explain why the oxygen level at the interface between the silicides and Si substrates is below the detection limit of SIMS for both samples (Fig. 8). Therefore, the interfacial oxygen, if ever introduced because of the variations of the preparation procedure for the Ti/Mo bilayer deposition, does not seem to stop the formation of $(Mo,Ti)Si_2$. The direct growth of the $C54$ phase of $TiSi_2$ is then guaranteed.

IV. CONCLUSIONS

It has been demonstrated that with the interposition of a thin layer of either Mo or Ta between Ti and Si, the $C54$ phase of $TiSi_2$ can be formed apparently without the need to go through the otherwise usual $C49-C54$ phase transformation. The formation of the hexagonal $(Mo,Ti)Si_2$ or $TaSi_2$ phase is found to be responsible for the easy, early formation of the $C54$ phase. Although the resistivity and preferential orientation of the $C54$ phase formed can depend on the preparation procedure used for the deposition of the metal layers, the template mechanism resulting in early growth of the $C54$ phase seems to be unaffected.

As the in-plane lattice match between the $C54$ phase of $TiSi_2$ and the template (crystalline) phase is of prime importance for template growth, a number of other phases such as $NbSi_2$ and $(W,Ti)Si_2$ (Ref. 31) can also be utilized for the purpose of enhancing the growth of the $C54$ phase. However, caution should be exercised in choosing a new metal system and at least two properties need to be examined: compound formation within the new metal system in contact with Si and the mobility of the metals involved in comparison with Si.

The template mechanism may also be operative in the experiments with ion implantation of Mo or W into Si prior to Ti deposition.[10,14] A continuous layer of $(Mo,Ti)Si_2$ or $(W,Ti)Si_2$ does not have to be a prerequisite for the enhanced formation of the $C54$ phase. Small particles of these ternary phases spread over the interface between the Ti layer and the Si substrate can act as seeds for the nucleation of the $C54$ phase. Whether this hypothetical mechanism is true remains to be investigated.

ACKNOWLEDGMENTS

The authors wish to thank M. Jargelius for TEM analysis, J. Cardenas for SIMS measurement, N. Lundberg for RBS data acquisition, and N.-O. Ersson for XRD analysis. A.M. is a grant holder of the European program Training and Mobility of Researchers (TMR). This work was financially supported by the Swedish Board for Technical and Industrial Development (NUTEK).

*Electronic address: aliette@ele.kth.se

[1] F. M. d'Heurle, P. Gas, I. Engström, S. Nygren, M. Östling, and C. S. Petersson, IBM Res. Rep. RC 11151, No. 50067, 1985 (unpublished).

[2] R. Beyers and R. Sinclair, J. Appl. Phys. **57**, 5240 (1985).

[3] M.-L. Rostoll, D. Maury, J.-L. Regolini, M. Haond, P. Delpech, P. Gayet, and M. LeContellec, in *Proceedings of the 26th European Solid State Device Research Conference*, edited by G. Baccarani and M. Rudan (Editions Frontieres, 1996), p. 93.

[4] R. Beyers, D. Coulman, and P. Merchant, J. Appl. Phys. **61**, 5110 (1987).

[5] H. Jeon, C. A. Sukow, J. W. Honeycutt, G. A. Rozgonyi, and R. J. Nemanich, J. Appl. Phys. **71**, 4269 (1992).

[6] J. B. Lasky, J. S. Nakos, O. J. Cain, and P. J. Geiss, IEEE Trans. Electron Devices **38**, 262 (1991).

[7] J. A. Kittl, Q. A. Prinslow, P. P. Apte, and M. F. Pas, Appl. Phys. Lett. **67**, 2308 (1995).

[8] K. L. Saenger, J. C. Cabral, Jr., L. A. Clevenger, R. A. Roy, and S. Wind, J. Appl. Phys. **78**, 7040 (1995).

[9] R. Achutharaman, P. Hey, and J. L. Regolini, Semicond. Int. **19**, 149 (1996).

[10] R. W. Mann, G. L. Miles, T. A. Knotts, D. W. Rakowski, L. A. Clevenger, J. M. E. Harper, F. M. d'Heurle, and C. Cabral, Jr., Appl. Phys. Lett. **67**, 3729 (1995).

[11] A. Mouroux, S.-L. Zhang, W. Kaplan, S. Nygren, M. Östling, and C. S. Petersson, Appl. Phys. Lett. **69**, 975 (1996).

[12] A. Mouroux, S.-L. Zhang, W. Kaplan, S. Nygren, M. Östling, and C. S. Petersson, in *Advanced Metallization for Future ULSI*, edited by K. N. Tu, J. W. Mayer, J. M. Poate, and L. J. Chen, MRS Symposia Proceedings No. 427 (Materials Research Society, Pittsburgh, 1916), p. 511.

[13] C. Cabral, L. A. Clevenger, J. M. E. Harper, F. M. d'Heurle, and K. L. Saenger, J. Mater. Res. **12**, 304 (1997).

[14] L. A. Clevenger, R. W. Mann, G. L. Miles, J. M. E. Harper, F. M. d'Heurle, C. Cabral, Jr., K. L. Saenger, T. A. Knotts, and D. W. Rakowski, IBM Res. Rep. RC 20073, No. 88794, 1995 (unpublished).

[15] W. Kaplan, A. Mouroux, S.-L. Zhang, and S. Petersson, Microelectron. Eng. (to be published).

[16] Standard JCPDS diffraction pattern 6-607 [hexagonal $(Ti_{0.4}Mo_{0.6})Si_2$], JCPDS-International Center for Diffraction Data, RDF-2 Database, 12 Campus Boulevard, Newton Square, PA 19073-3273, USA.

[17] Standard JCPDS diffraction pattern 7-331 [hexagonal $(Ti_{0.8}Mo_{0.2})Si_2$], JCPDS-International Center for Diffraction Data, PDF-2 Database, 12 Campus Boulevard, Newton Square, PA 19073-3273, USA.

[18] Standard JCPDS diffraction pattern 35-785 (orthorhombic $TiSi_2$), JCPDS-International Center for Diffraction Data, PDF-2 Database, 12 Campus Boulevard, Newton Square, PA 19073-3273, USA.

[19] F. M. d'Heurle, in *VLSI Science and Technology*, edited by C. Dell'Oca and W. M. Bullis (The Electrochemical Society, Pennington, 1982), pp. 194–212.

[20] Standard JCPDS diffraction pattern 38-483 (hexagonal $TaSi_2$) JCPDS-International Center for Diffraction Data, PDF-2 Database, 12 Campus Boulevard, Newton Square, PA 19073-3273, USA.

[21] Standard JCPDS diffraction pattern 8-450 (hexagonal $NbSi_2$), JCPDS-International Center for Diffraction Data, PDF-2 Database, 12 Campus Boulevard, Newton Square, PA 19073-3273, USA.

[22] JCPDS-International Center for Diffraction Data, PDF-2 Database, 12 Campus Blvd., Newton Square, PA 19073-3273.

[23] *Pearson's Handbook of Crystallographic Data for Intermetallic Phases*, edited by P. Villars and L. D. Calvert (American Society for Metals, Metals Park, Ohio, 1985).

[24] C. D. Capio, D. S. Williams, and S. P. Murarka, J. Appl. Phys. **62**, 1257 (1987).

[25] R. Dahan, J. Pelleg, and L. Zevin, J. Appl. Phys. **67**, 2885 (1990).

[26] M.-A. Nicolet and S. S. Lau, in *VLSI Electronics, Microstructure Science*, edited by N. G. Einspurch and G. B. Larrabee (Academic, New York, 1983), p. 360.

[27] F. M. d'Heurle, J. Mater. Res. **3**, 167 (1988).

[28] L. J. Chen and K. N. Tu, Mater. Sci. Rep. **6**, 53 (1991).

[29] Standard JCPDS diffraction pattern 17-917 (hexagonal $MoSi_2$), JCPDS-International Center for Diffraction Data, PDF-2 Database, 12 Campus Boulevard, Newton Square, PA 19073-3273, USA.

[30] R. Beyers, J. Appl. Phys. **56**, 147 (1984).

[31] P. Gas, F. J. Tardy, and F. M. d'Heurle, J. Appl. Phys. **60**, 193 (1986).